WHOI-2006-14

Woods Hole Oceanographic Institution

Initial Results from a Cartesian Three-Dimensional Parabolic Equation Acoustical Propagation Code

by

Timothy F. Duda

Woods Hole Oceanographic Institution
Woods Hole, MA 02543

December 2006

Technical Report

Funding was provided by the Office of Naval Research under Contract No. N00014-05-1-0482.

WHOI-2006-14

Initial Results from a Cartesian Three-Dimensional Parabolic Equation Acoustical Propagation Code

by

Timothy F. Duda

December 2006

Technical Report

Funding was provided by the Office of Naval Research under Contract No. N00014-05-1-0482.

Approved for Distribution:

James F. Lynch Chair

Department of Applied Ocean Physics & Engineering

Initial Results from a Cartesian Three-Dimensional Parabolic Equation Acoustical Propagation Code

Timothy F. Duda
Applied Ocean Physics and Engineering Department
Woods Hole Oceanographic Institution
Woods Hole, MA 02543

Abstract

A three-dimensional (3D) parabolic equation acoustical propagation code has been developed and run successfully. The code is written in the MATLAB language and runs in the MATLAB environment. The code has been implemented in two versions, applied to

(1) Horizontal low-frequency (100 to 500 Hz) propagation through the shallow water waveguide environment;
(2) Vertical high-frequency propagation (6 to 15 kHz) to study normal-incidence reflection from the lower side of the ocean surface.

The first edition of the code reported on here does not implement refinements that are often found in 2D propagation models, such as allowing density to vary, optimally smoothing sound-speed discontinuities at the water/seabed interface, and allowing an omni-directional source. The code is part of a development effort to test the applicability of 2D (and N by 2D) models, which have more refinements than this model, to the study of fully 3D propagation problems, such as sound transiting steep nonlinear coastal-area internal waves and/or sloping terrain, and to provide a numerical tool when the full 3D solution is needed.

Introduction

A computational code has been implemented to study truly three-dimensional acoustical propagation. The code and some initial results obtained with the code are described here. The method that is employed is the split-step Fourier (SSF) solution of the parabolic acoustic wave equation (PE) [1, 2]. The equation describes one-way solutions for waves propagating from a monochromatic source. So-called marching algorithms can be used to find the steady-state one-way solutions. The SSF technique divides propagation over each distance increment through a heterogeneous sound speed (refractive index) environment into step-by-step "free space" propagation through a medium having a fixed wavenumber (usually related to a fixed sound speed, often the mean), and periodically introduced (at each step) phase fluctuations consistent with departures from that fixed speed. The free space propagation is handled in the wavenumber domain, and the phase anomalies are introduced in the spatial domain. Amplitude effects such as absorption are introduced with the phase anomalies. Thus, each step requires a Fourier transform and an inverse Fourier transform, with the spatially marched complex acoustic field solution Ψ given by

$$\Psi(x+\delta) = \mathbf{F}^{-1}\left[G \cdot \left(\mathbf{F}\left[P \cdot \Psi(x) \right] \right) \right]$$

where $P = A_P \exp(-ik_0 U \delta)$ is the phase (and amplitude) operator in the spatial domain, G is the propagator in the wavenumber domain, $\mathbf{F}$ is the Fourier transform operator, $U = (c - c_0) / c_0$, c_0

is a reference sound speed and c is sound speed, $k_0 = \omega / c_0$ is wavenumber, ω is frequency, and δ is the distance increment in the x direction.

In ocean acoustics, the PE is usually implemented in vertical slices (vertical planes). At each step, the vertical dimension and the vertical wavenumber form the transform variable pair. A few 2D SSF PE implementations are available, including the Monterey-Miami PE and the University of Miami PE which preceded it. These methods utilize single-dimension fast Fourier transforms (FFTs). For horizontal propagation, these methods implement the surface boundary condition with an out-of phase image source in an image domain on the opposite side of the surface from the water and seafloor, meaning that the numerical domain size is twice that of the modeled water-column and the modeled portion of the sea floor.

The extension of the 2D SSF PE method to a Cartesian coordinate 3D environment primarily involves changing from a 1D to a 2D Fourier transform. This adds substantially to the calculation time required to cover a specific distance and depth of water at a specific grid resolution. In addition to the added run time, larger amounts of memory are also required to perform the calculation. The code reported on here uses the aforementioned image-domain 2-D FFT technique. The wide-angle variant of the propagation operator is used [2]. The aspect ratio of the vertical and horizontal grid intervals is adjustable, as is the domain size, the dimensions of the FFT, and the propagation step length. This code originates from 3D propagation codes used for optical studies [3,4]. A trial MATLAB®* version was written by John Colosi, from which this code was derived.

Note that a different 3D PE code, FOR3D, has been used for some years in ocean acoustics, perhaps most recently by Naval Research Laboratory investigators [5,6]. FOR3D uses a range-azimuth computational grid and implements narrow-angle azimuthal coupling.

There are number of issues still to be resolved in order to apply the technique in a reliable fashion to ocean acoustics problems. One unknown is the grid resolution needed to ensure a good solution. The definition of a source field and source level has not yet been resolved. Finally, the required absorption of sound at the lateral edges is being investigated. Progress on these in two distinct implementations is described here, and example solutions are shown. The two implementations are 100-500 Hz propagation up to 10's of kilometers in a shallow water waveguide, and o(10 kHz) upward then downward vertical propagation with a reflection at the rough (wavy) sea surface intended to model signals from inverted echo sounders..

Shallow Water Waveguide

Code for modeling the coastal shallow-water waveguide has been completed. Some preliminary results are shown here. All results shown in this section are for 400-Hz propagation. Grid sizes of 1024 × 1024 and 2048 × 2048 have been used. The propagation step used here is two acoustic wavelengths (λ) in length (7.5 m in this case). The terminology here is that propagation is in the x direction, with y being the horizontal dimension normal to propagation. The domain size in y that has been used is 300 wavelengths, so that there are about 3.4 or 6.8 grid points per wavelength of sound. (This was chosen after non-exhaustive testing.) The vertical dimension has higher resolution, with an adjustable aspect ratio A. The results shown here use an aspect ratio $A = 4$. Thus, because of the domain mirroring about the surface, the vertical domain is $300/2A = 75$ wavelengths. The source can be positioned at any depth at $y = 0$.

* MATLAB® is a high-level language and interactive environment produced by The MathWorks, Inc.

For the results shown here the source has a Gaussian profile in z and y with scale length of 1.25 m. It produces an axisymmetric beam with a width of about 20°. More recently a Green's function starting field has been implemented. An absorbing boundary is required to prevent sound wrap around and aliasing in the domain. This is done in a manner similar to the seafloor attenuation. A smooth function that shrinks from unity in the center of the domain to near zero at the edge is applied at each edge of the domain as a factor of A_P. The function for each edge is

$$A_{EN} = \exp\left(-\beta\delta \exp\left(-\left(D/\alpha Y \right)^2 \right) \right)$$

where δ is the step length in the propagation (x) direction, Y is one/half the domain width, D is the distance from the nearest edge. Parameter values used successfully with 400 Hz, $\delta = 2\lambda$. are $\alpha = \lambda/50$ and $\beta = 2.1$. The function defined over the entire domain A_E is composed of the sum of four A_{EN}. The formula is written to be compatible with the Colosi code but not with the Martin/Flatté code, which implemented a radial attenuation function. Successful runs without leakage out of the domain (particularly in the y direction, rather than z) depend on careful choice of α and β. The numbers given here are for a $y = 300\ \lambda$ domain, 400 Hz, and $\delta = 2\lambda$, and may not be suitable for other situations. Algorithms to automatically produce suitable parameters based on physical principles need to be developed and implemented.

Attenuation in the seafloor is introduced by including a factor A_B in the medium-anomaly phase fluctuations at each step. This is done by appropriately reducing the magnitude of bottom-location complex phase-screen elements below unity, as with A_E. That is, the field is multiplied by $P = A_E\, A_B \exp(i\varphi)$ at each step, with A_B less than one in the bottom and φ determined by the fluctuating sound-speed of the medium.

Propagation is modeled with domain depths of 60 m and 80 m. Background sound speed in the water column *c(z)* has a three-layer form, with fixed *dc/dz* in each layer. The sound speed values that define the layers are *c=1522* m/s at the surface, 1520 at 15 m depth, 1484 at 30 m, and 1481 at the bottom. Seafloor sound-speed is 1650 m/s at the interface, increasing with a gradient of 1 m/s per meter below the seafloor. Attenuation in the seafloor is 0.1 db/wavelength.

Most of the test runs include time-frozen nonlinear wave-type thermocline displacements added to the background *c(z)*. These have the form of permanent wave solutions of the Korteweg-deVries equation, given by the formula $\eta = \eta_0\, \mathrm{sech}^2((\xi-\xi_0) / L)$, where ξ is distance in the direction of travel of the nonlinear wave, L is the half width, and η_0 is the maximum displacement (the amplitude). As appropriate for numerical input, wave dimensions are stretched in domain slices (across the wave) that lie normal to the propagation direction.

Run time is 1700 sec for a range of 10 km (1024^2 FFT, 1333 steps, 9997.5 m) on a 2.8 GHz Pentium-4 Windows PC with adequate memory (greater than 1 GB). Run time increases if interim fields are saved or more complex domains are input or computed algorithmically during the run.

Layered Environment

The first results shown here will be for a uniform layered environment with no internal waves. Figures 1 and 2 show the amplitude and phase of sound propagated using the 1024 × 1024 point option in the 60-m domain. Fields at ranges of 500 and 5000 m are shown. These show the effects of the y-boundary absorption and of spreading. The results appear as expected.

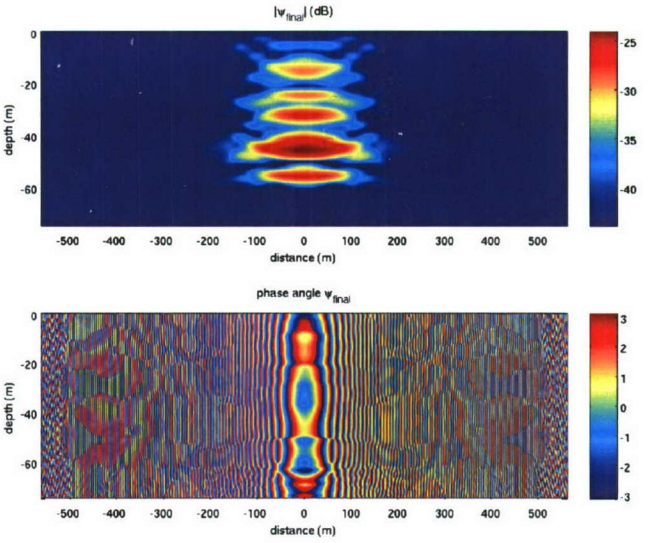

Figure 1. The acoustic field after 500-m propagation through the 60-m deep three-layer environment with no internal waves is shown. Intensity in the tangential cross-range plane is shown at the top, phase in the same plane at the bottom. The beam source has expanded to fill a lateral distance of 200 m, indicating a beam width of about 22 degrees.

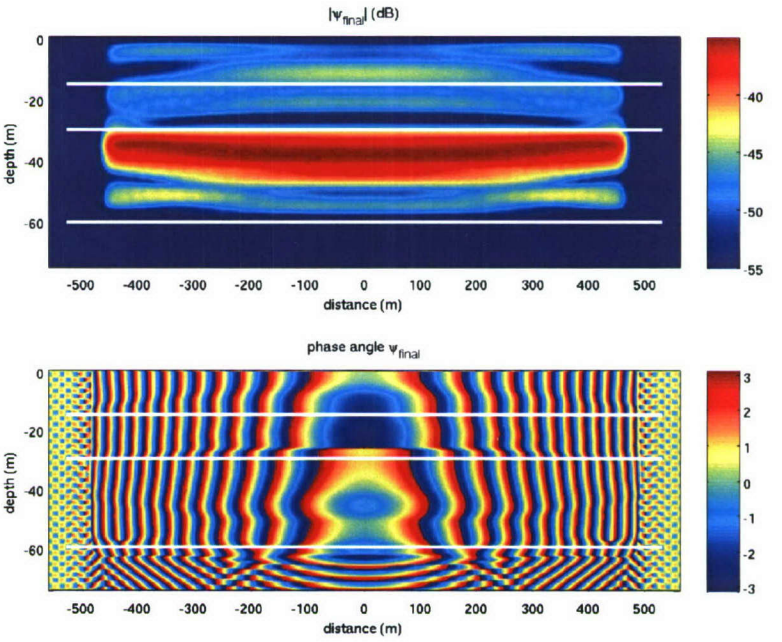

Figure 2. Acoustic field results for 5000-m propagation through the 60-m deep three-layer environment. This range is approximately twice that where the sound impinges on the lateral absorbing layers.

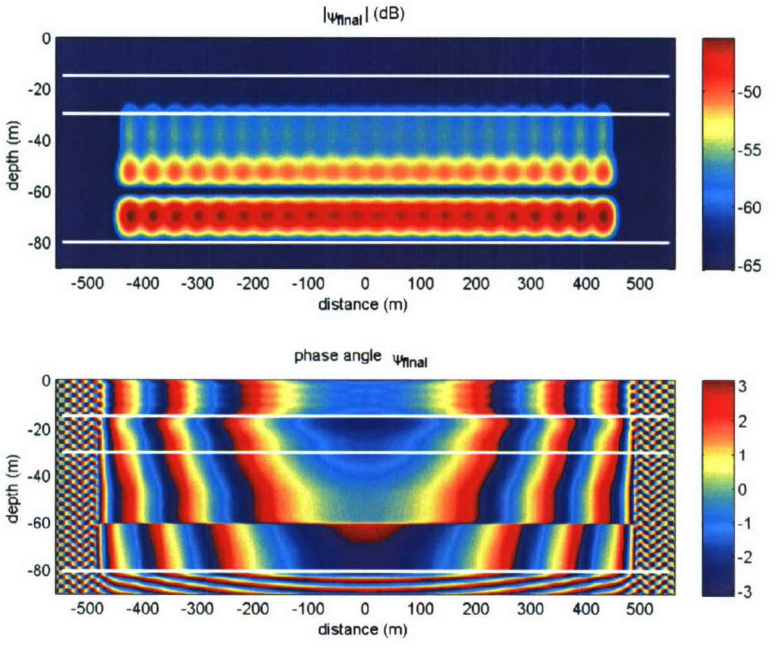

Figure 3. 400-Hz acoustic field after propagation of 20 km through the 80-m deep three-layer environment in 2λ steps is shown. The intensity shows a ripple.

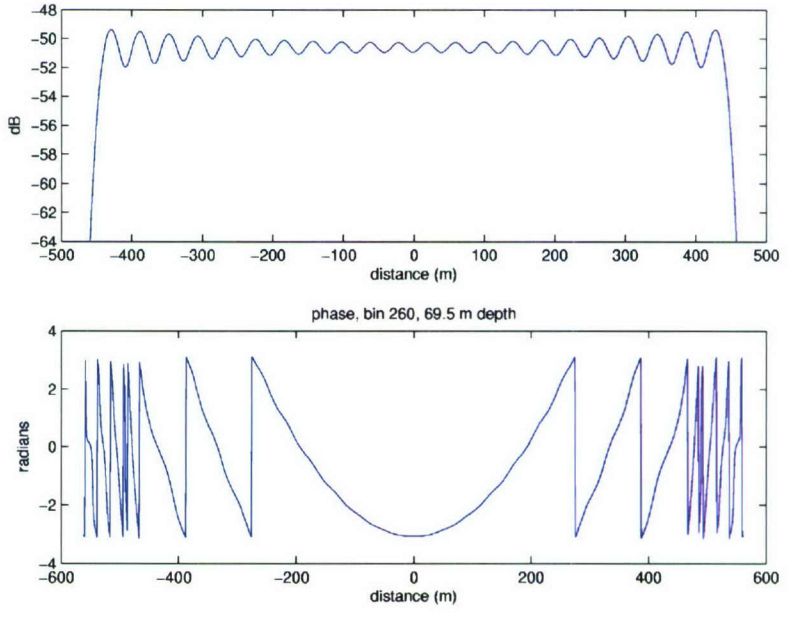

Figure 4. Intensity and phase at 69.5 m depth from the previous figure are plotted as functions of cross-range (y) distance.

Figure 3 shows results for 20-km propagation in the deeper domain. At this range, some spurious focusing occurs. This effect can be caused by the rather large range step size, and may also emanate from the edge absorption method. Figure 4 is a line drawing of amplitude and phase taken from Figure 3, more clearly showing the amplitude ripple.

Internal Wave Environments

Next, Figure 5 shows the acoustic field after propagation through an environment having an internal wave aligned to be consistent with motion in the y direction, so that there is no x dependence of the sound speed field. The y dependence of $c(x,y,z)$ can be seen in the figure. The phase plot has a minimum above the trough of the wave, indicating a maximum speed, as expected. The greater intensity to the right of the wave also indicates refraction by the wave. A meaningful way to express the acoustic effect under these conditions would be horizontal refraction of normal modes, with group speed maxima in the wave expelling the mode energy.

The fields shown thus far have been for environments with no x-direction variability. Now, results are shown for environments with range variability created by shifting the field $c(x=0, y, z)$ in the y-direction a fixed number of grid points for each range step, creating features having fixed angle ϕ with respect to the propagation path at $y = 0$. Figure 6 shows results for a field of two waves that move across and out the domain in the y direction, then re-entering the domain. The wave field $\eta(x,y)$ is shown in Figure 7.

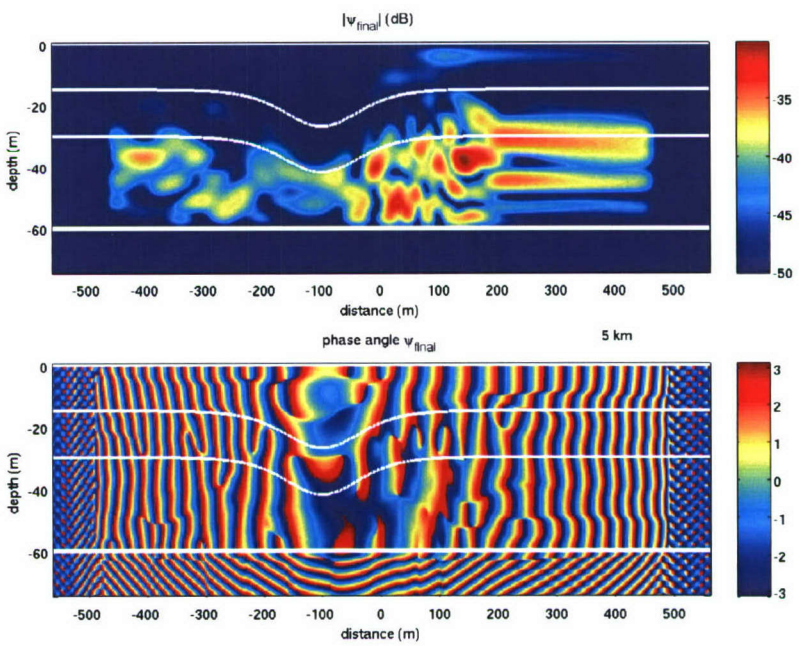

Figure 5. The acoustic field at distance 5000 m from the source is shown for the situation of propagation parallel to the crest of an internal wave with L=86 m and η_0 = 12 m. The 60-m depth environment is used. The boundaries of the two layers are drawn in this view looking in the direction of propagation (x), showing the fixed position of the internal wave in the cross-range direction (y). The source is at y = 0 and depth 40 m. Note the minimum of phase above the trough of the wave, and the larger intensity on the right caused by refraction away from the warm anomaly in the wave.

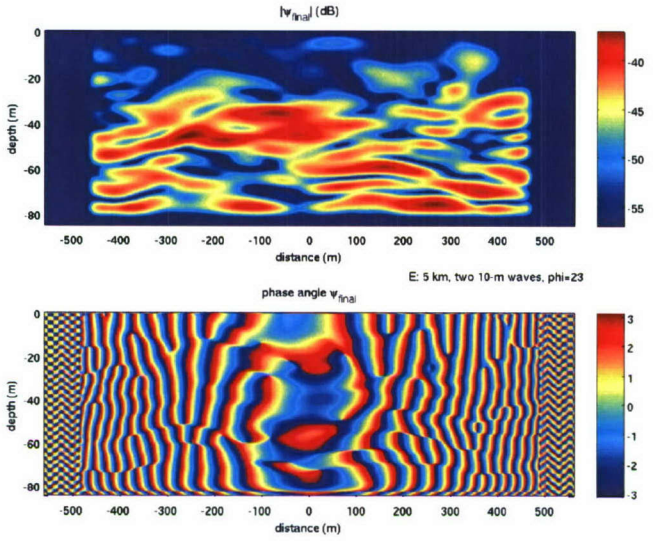

Figure 6. The field resulting from propagation through internal waves of 10-m amplitude and 95-m half width (L) at an angle of $\phi = 23.7°$. This is oblique acoustic propagation with respect to the wave troughs. Because the down-range half-width of the internal waves is 235 m, there is a strong possibility that coupled mode propagation is occurring. Adiabatic mode refraction of the type illustrated in Figure 5 is not expected to occur.

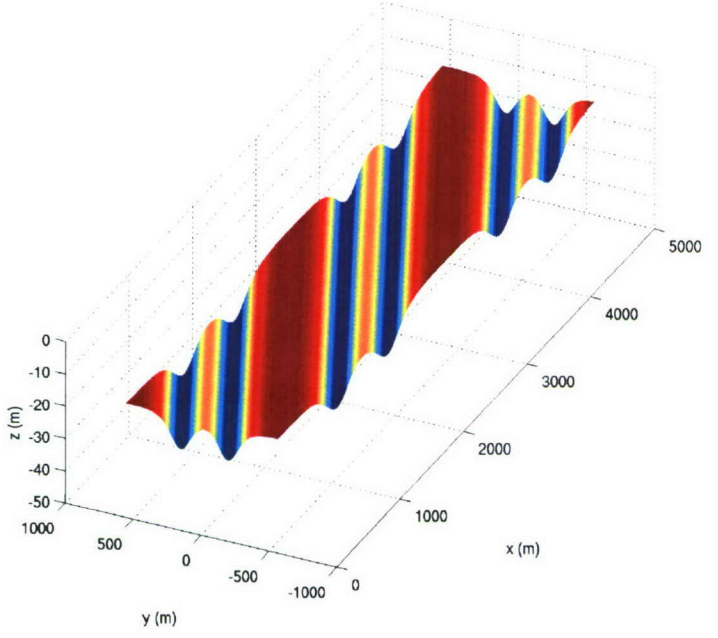

Figure 7. The internal wave environment used to generate the field of Figure 6 is shown. The depth of the top of the strong gradient layer is plotted versus x and y. Wave troughs are blue.

Figures 8-11 show results for simulations having one internal wave of η_0=10 m, L=95 m at 4950 m from the source at $y = 0$, with the wave at various angles ϕ. These are similar to the situation shown in Figure 7 except only one wave is present. The fields that result at the range of $x = 10$ km (Figures 8 and 9) have significant structure in y, as expected from either coupled mode or adiabatic propagation through media that have 3-D variability.

Figure 10 shows the depth-integrated range-normalized intensity (intensity times range) that results from waves at each of the two small angles of ϕ equal to 4° and 8°. The smaller angle case clearly shows refraction, the other does not, although the next figure will suggest that refraction also occurs. Figure 11 shows the differences between the fields of Figure 10 and control cases with no internal waves. In the top panel, the blue area below the 4° internal-wave position has depleted energy, with energy diverted into the beam near the wave seen at the top. The same effect can be seen in the lower panel for the 8° wave. Each of the panels also shows azimuthal energy dependence appearing as a few beams. The beams are green, separated by blue areas of energy depletion. This effect is caused by source to internal-wave distance being a function of azimuth, causing azimuthal variations in mode coupling, and subsequent variations in energy loss via bottom interaction [7].

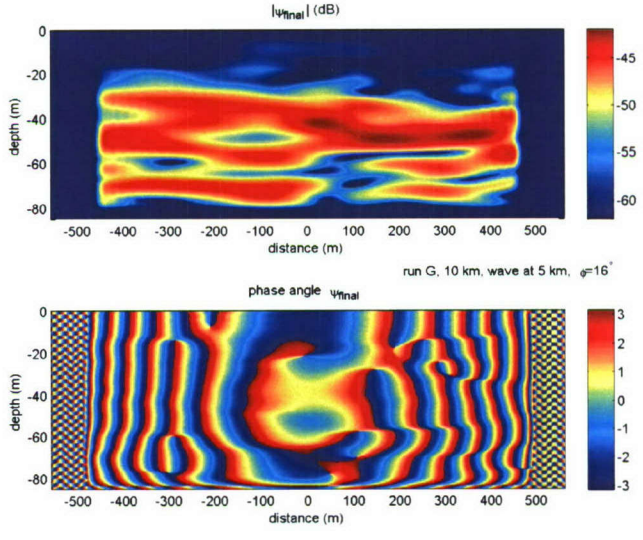

Figure 8. The intensity and phase at the 10-km range end-plane for the case of one internal wave 5 km from the source (measured at y = 0). The internal wave is at angle $\phi = 16°$. This is a situation that shows no evidence of horizontal deflection. The phase minimum is at the point closest to the source, which is y = 0 in the center of the figure.

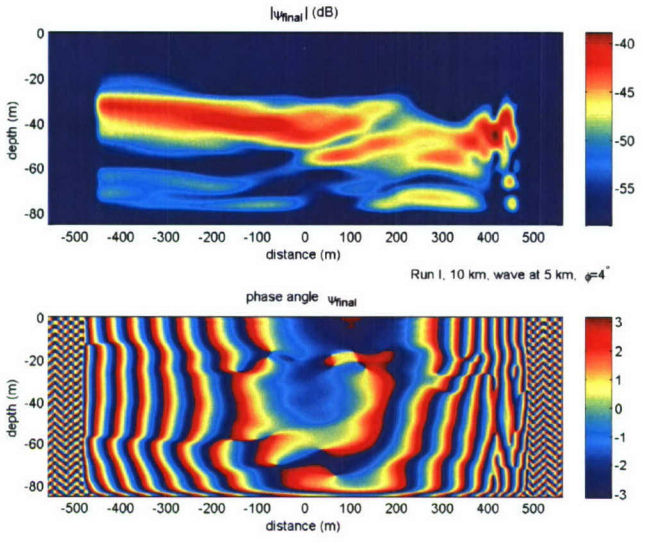

Figure 9. Intensity and phase are shown for a situation similar to that of the previous figure, except the wave angle is $\phi = 4°$. This situation shows horizontal refraction of the sound. The depth-averaged sound intensity is not symmetric around $y = 0$, unlike the $\phi = 16°$ case (not shown). The phase minimum is not at $y = 0$.

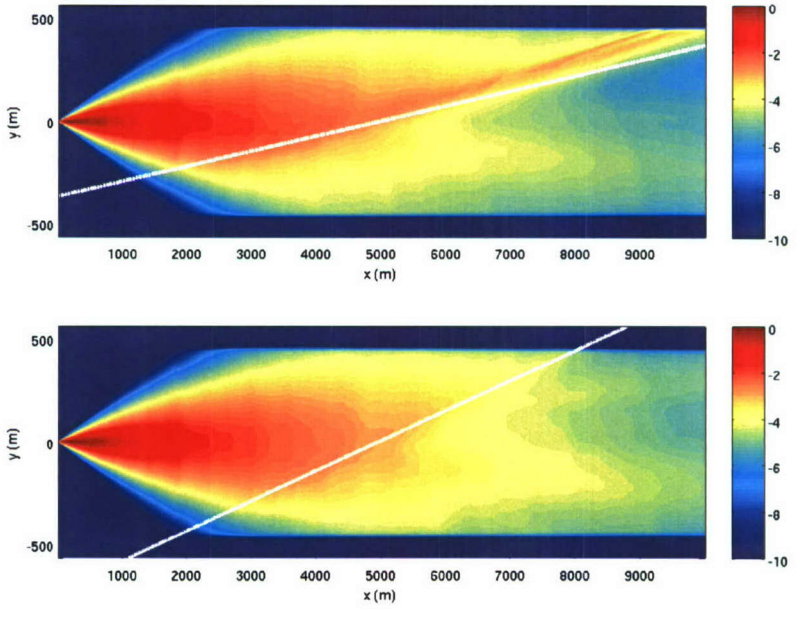

Figure 10. The depth-averaged range-normalized intensity is shown in plan view for two cases, each with a single internal wave 4950 m from the source at $y = 0$. (Upper panel) The wave has $\phi = 4°$. (Lower panel) The wave has $\phi = 8°$. The trough of the wave is shown in each panel in white. The effects of refraction are clearly seen in the upper panel. [The 8° wave situation shows slight azimuthal dependence of the energy, the result of weak horizontal refraction and possibly also altered bottom attenuation effects resulting from mode coupling.]

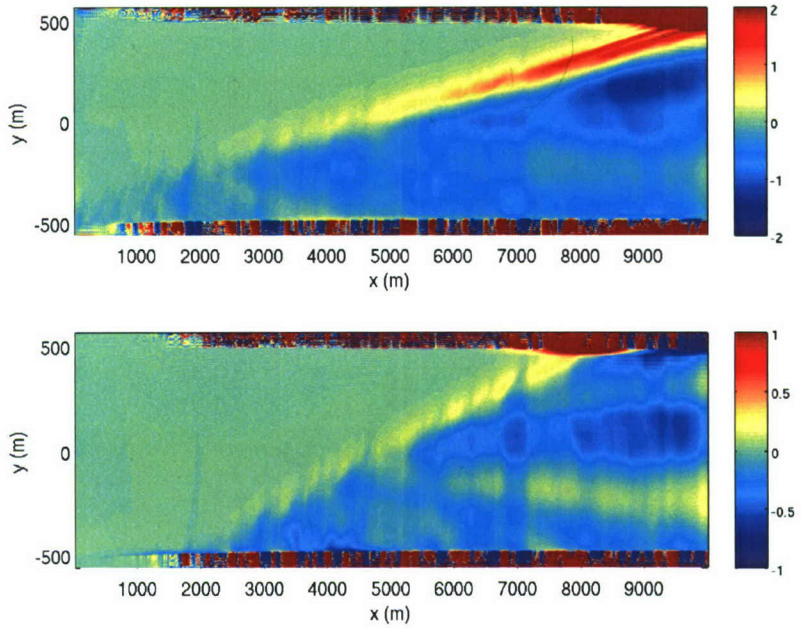

Figure 11. The differences of the fields of the previous figure with the no internal wave case are plotted. The intensity scales differ in the two plots. Amplification along the wave caused by refraction is seen in both cases. Positive values in the refracted beam in the upper image are clipped.

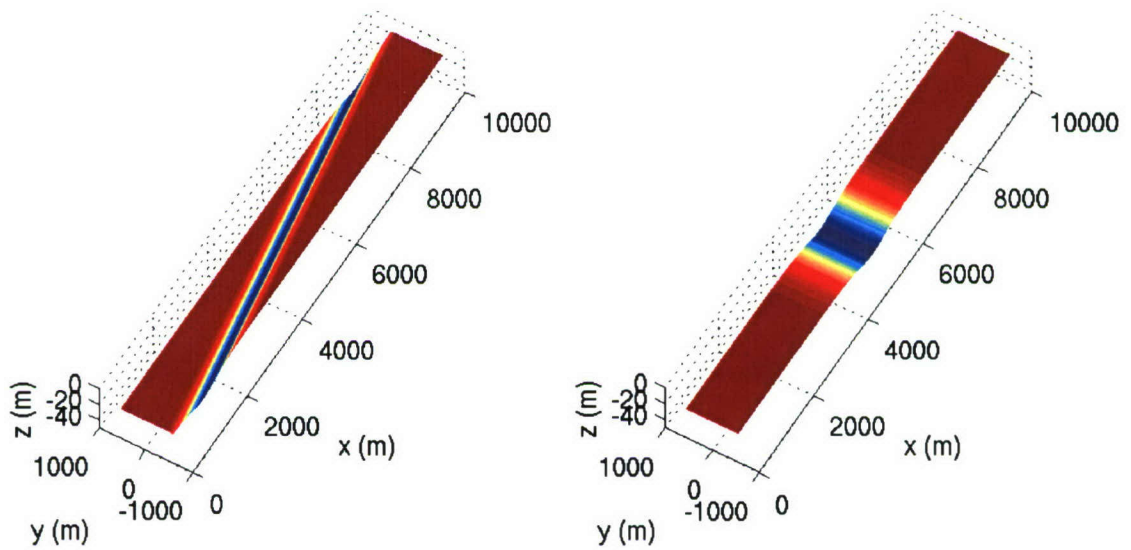

Figure 12. Two related environments are shown in the format of Figure 7. These are identical along the line y = 0. On the left is a strongly azimuthally varying field with a single wave at angle $\phi = 8°$; on the right is the weakly azimuthally varying case generated by using the y = 0 field at all y.

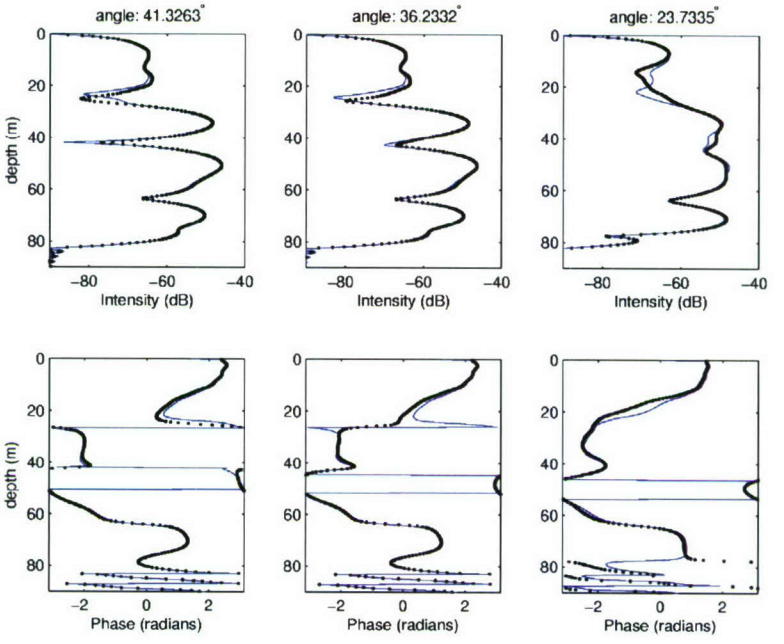

Figure 13. 3-D to pseudo-2-D comparison for various angles of waves. At the final range of x = 10 km and y = 0, intensity is shown above, phase below. The internal waves all have amplitude 10 m, horizontal scale L = 95 m. The most pronounced discrepancy that is seen, at $\phi = 23°$, is unexplained.

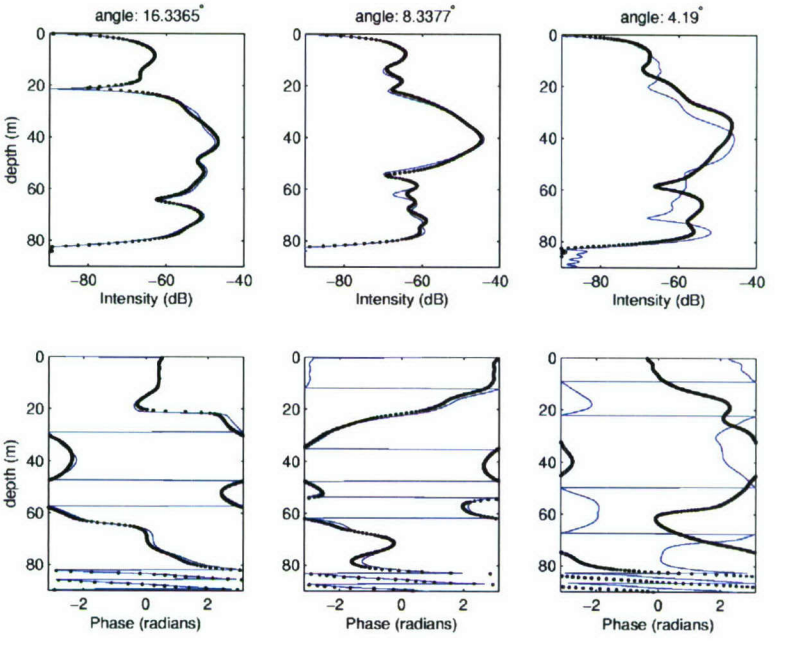

Figure 14. Additional 3-D to pseudo-2-D comparisons for 10:95 waves. The $\phi = 4°$ case shows a clear difference, indicating refractive effects, the others do not.

3-D to 2-D comparison

The accuracy of $N \times$ 2D simulations of propagation through 3D environments, such as in previous work [7], can be evaluated using the 3D model. To avoid discrepancies cause by comparing codes, we perform such an evaluation by comparing results from strongly-varying and weakly azimuthally varying 3D environments that are identical along the line $y = 0$. Two environments of this type are shown in Figure 12.

Using environment pairs of the type shown in Figure 12 the 3D to 2D comparison is made for single 10-m amplitude, $L = 95$ m waves of depression propagating at various angles. Figures 13 and 14 show that the 2D simulations give very accurate results for internal waves having crests (or troughs) at angle 8 degrees or greater from the direction of propagation. These are the same situations that show little refractive influence on intensity.

Mode Coupling

The process of coupled mode propagation has been demonstrated to occur when sound in waveguides similar to that modeled here encounters internal waves of the type used here. Figure 15 shows that this is indeed occurring for a wave at angle $\phi = 30.4°$. The modeled wave has $a =$ 10 m and $L = 95$ m as previously, which has a wave scale of 188 m along $y = 0$. This case is expected to have mode coupling [8], verified by the modal decomposition of the field as a function of x shown in the figure.

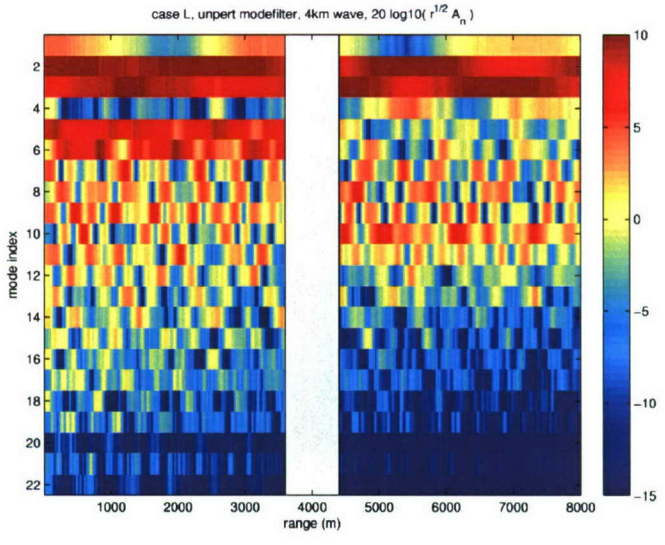

Figure 15. The magnitudes of mode coefficients times range$^{1/2}$ are computed along $y = 0$ for a case similar to those shown earlier (400 Hz, source depth 40 m, one 10:95 nonlinear internal wave). The internal wave is at angle 30.4° with position $x = 4000$ m at $y = 0$. Mode filtering is performed with mode functions (computed using the code FEMODE.F from Naval Research Lab.) for the unperturbed environment, i.e. outside the wave. The area within the wave where these are not the correct mode functions is shown in gray. Modes should be uncoupled outside the wave, so the oscillations in range of the coefficients show small numerical errors known to be associated with overly long range step increment. Despite this, mode coupling in the wave, which is expected, can be seen to strip energy from modes 5 and 6.

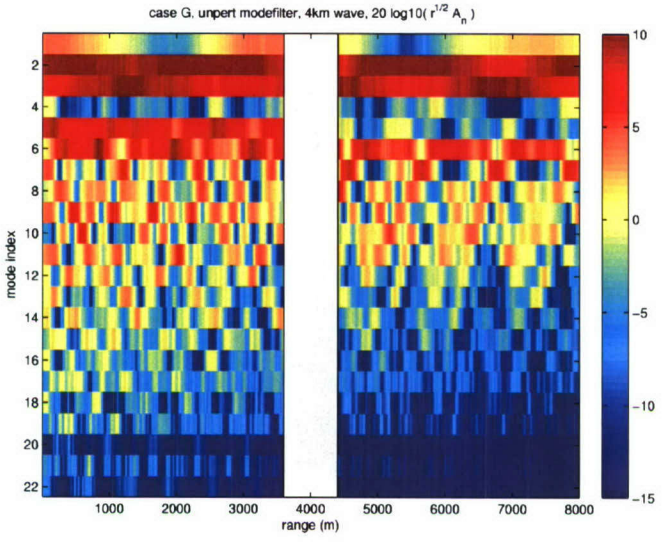

Figure 16. A result similar to that of the previous figure is shown, with the exception that the wave angle is 16 degrees. The internal wave scale projected onto a radial line of propagation at $y = 0$ is $L_p = 95/\sin\phi = 344$ m.

For decreasing wave angle ϕ the scale of the internal waves projected onto radial lines of propagation becomes quite large, which reduces lateral gradients and weakens the mode coupling effect [8]. Figure 16 shows that despite this trend, a wave at angle 16 degrees which has an effective wave scale near 350 m along the propagation path still causes significant coupling, with mode 5 severely depleted after traversal of the wave.

Vertical Channel: PIES surface reflection simulation

Propagation of high-frequency sound (6 to 15 kHz) emitted from a bottom-mounted PIES instrument to the ocean surface and then back to the bottom has also been modeled. A uniform sound speed has been used throughout, enabling an analytic field to be applied at the surface, reducing the computation by 50 percent. Upward-propagation test runs reproduced the phase calculated using spherical spreading with high accuracy. The surface reflection is done with a phase-screen treatment; at each point, the field is multiplied by $P = \exp(i\varphi)$, with phase of $\varphi = 4\pi h/\lambda$. The test simulations typically used 32-λ steps, 400-λ domain widths for the 1024×1024 point grid, and 800-λ domains for 2048×2048 point grids. The edge attenuation functions have different coeffecients from the low-frequency case, with $\beta = 8/\delta$ for the wide case with more grid points, double its value for the other case. The value $\alpha = \lambda/2$ is used.

Figure 17 shows the surface wave field that was used. This is computed by starting with a Pierson-Moskowitz spectrum with noise added, also having an azimuthal taper. This is Fourier transformed into the spatial domain. The field is self-similar at the wavelengths near the Fresnel scale that are important to the acoustics ($R_f^2 = D\lambda$ where D is depth), so the field is merely stretched to fit domains of different sizes for these test runs.

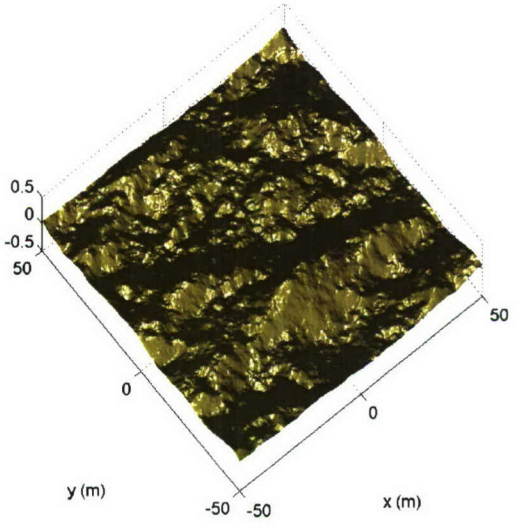

Figure 17. The gravity wave field at the surface used in the PIES vertical channel simulations.

Fields that result at the bottom in 512-m depth for 12 kHz are shown in Figure 18. Two different step sizes are used, showing restrictions on the SSF PE in a narrow domain. Short steps are required to avoid aliasing. This is not a problem for the shallow-water waveguide because short steps (relative to wavelength) are needed to model the highly-variable medium in the lower frequency case, shorter than would otherwise be needed. The vertical channel can be relatively uniform, but this can not be taken advantage of with very long steps because of the aliasing. Considering the acoustic field, note the intense focus (with interference pattern) in the lower part of Figure 18 that appears beneath the concave (from below) surface wave crest. Figures 19 and 20 show interesting patterns at 10 kHz for water depths of 3000 and 512 m, respectively.

Future Work

A number of enhancements would improve the code and would make simulation results more suitable for research purposes. These are listed here.

1. The density must be allowed to change. This can be done by changing the operator P which is applied in the spatial domain. This has been implemented but not fully tested. Methods for this are discussed in the literature [9].
2. Theoretical restrictions for the grid spacing and the step length should be computed as a function of frequency, and user-generated grids should be tested for compliance.
3. An algorithm is needed to automatically generate an effective edge absorption function, defined in terms of the grid spacing and the step increment. An entirely new function might be in order.

With these improvements the code will give more reliable results and will be suitable for studying 3D propagation in arbitrarily complicated environments. The code can already handle any water column and bathymetric conditions, although the input scheme for complicated environments has not been settled upon.

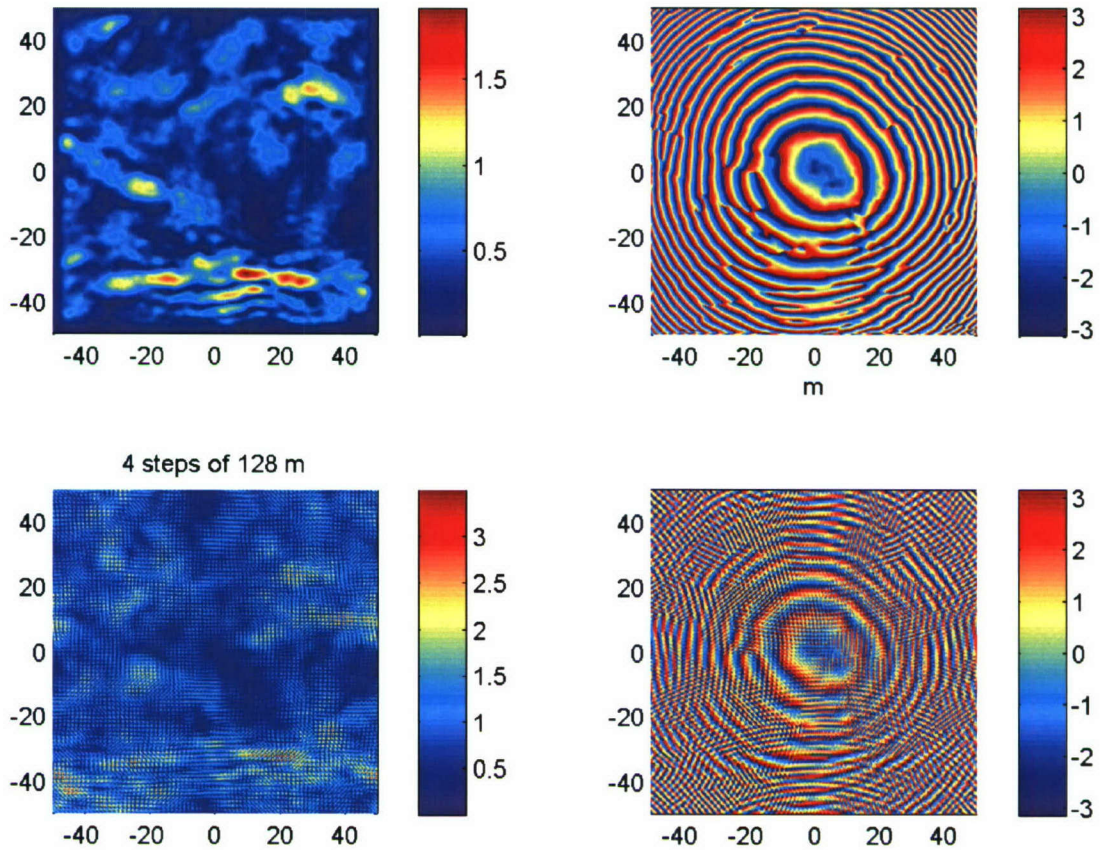

Figure 18. Edge absorption test for the vertical propagation channel. Results are compared for 128 4-m steps (top) versus 4 128-m steps (bottom). Amplitude is shown on the left, phase on the right. The propagator moves sound through the boundaries in the long-step case, causing aliasing.

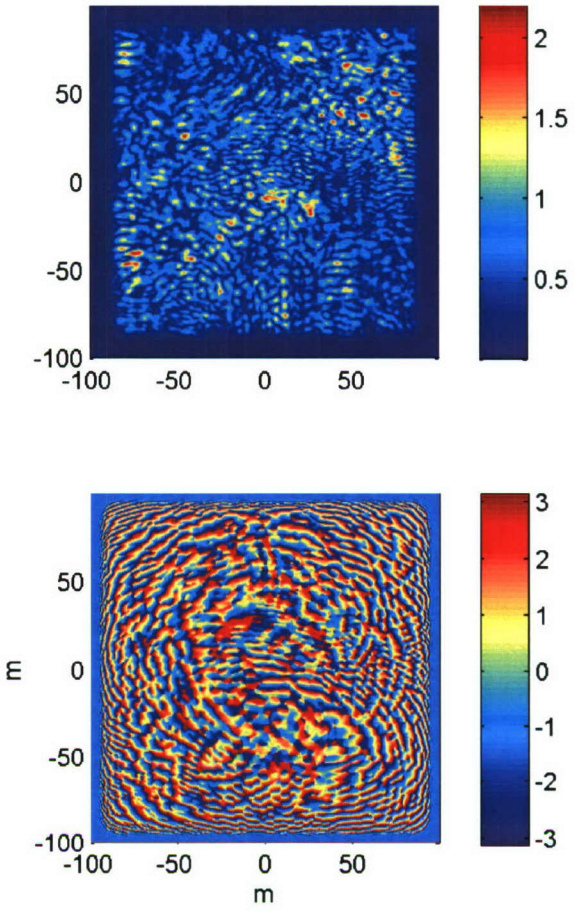

Figure 19. Acoustic amplitude (top) and phase (bottom) for a 10-kHz simulation of a surface reflected field from a bottom-mounted PIES in 3000-m depth water. 2048 x 2048 domain.

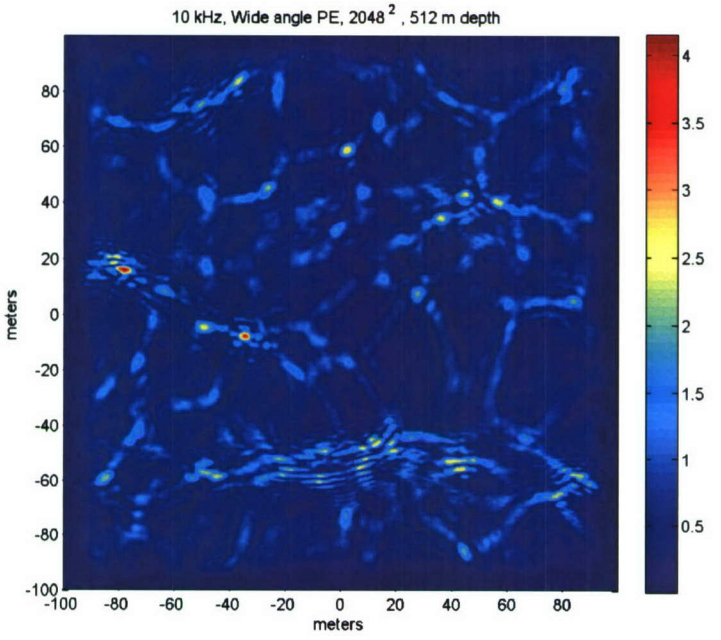

Figure 20. Intensity resulting from a wide-angle PE run vertically upward and back in 512 m depth water. The frequency is 10 kHz, and the surface waves are as shown in Figure 17.

References

[1] Hardin, R. H., and F. D. Tappert, Applications of the split-step Fourier method to the numerical solution of nonlinear and variable coefficient wave equations, *SIAM Rev., 15,* 423, 1973.

[2] Thomson, D. J., and N. R. Chapman, A wide-angle split-step algorithm for the parabolic equation, *J. Acoust. Soc. Am., 74*, 1848-1854, 1983.

[3] Martin, J. M., and S. M. Flatté, Intensity images and statistics from numerical simulation of wave propagation in 3-D random media, *Applied Optics, 27,* 2111-2126, 1988.

[4] Martin, J. M., and S. M. Flatté, Simulation of point-source scintillation through three-dimensional random media, *J. Opt. Soc. Am., 7,* 838-847, 1990.

[5] Oba, R., and S. Finette, Acoustic propagation through anisotropic internal wave fields: Transmission loss, cross-range coherence, and horizontal refraction, *J. Acoust. Soc. Am., 111*, 769-784, 2002.

[6] Finette, S., and R. Oba, Horizontal array beamforming in an azimuthally anisotropic internal wave field, *J. Acoust. Soc. Am., 114*, 131-144, 2003.

[7] Duda, T. F., Temporal and cross-range coherence of sound traveling through shallow-water nonlinear internal wave packets, *J. Acoust. Soc. Am., 119*, 3717-3725, 2006.

[8] Preisig, J. C, and T. F. Duda, Coupled acoustic mode propagation through continental-shelf internal solitary waves, *IEEE. J. Oceanic Eng., 22*, 256-269, 1997.

[9] Yevik, D., and D. J. Thomson, A hybrid spilt-step/finite difference PE algorithm for variable-density media, *J. Acoust. Soc. Am., 101*, 1328-1335, 1997.

50272-101

REPORT DOCUMENTATION PAGE	1. REPORT NO. WHOI-2006-14	2.	3. Recipient's Accession No.

4. Title and Subtitle
Initial Results from a Cartesian Three-Dimensional Parabolic Equation Acoustical Propagation Code

5. Report Date
December 2006

6.

7. Author(s) Timothy F. Duda

8. Performing Organization Rept. No.

9. Performing Organization Name and Address
Woods Hole Oceanographic Institution
Woods Hole, Massachusetts 02543

10. Project/Task/Work Unit No.

11. Contract(C) or Grant(G) No.
(C) N00014-05-1-0482
(G)

12. Sponsoring Organization Name and Address
Office of Naval Research

13. Type of Report & Period Covered
Technical Report

14.

15. Supplementary Notes
This report should be cited as: Woods Hole Oceanog. Inst. Tech. Rept., WHOI-2006-14.

16. Abstract (Limit: 200 words)

A three-dimensional (3D) parabolic equation acoustical propagation code has been developed and run successfully. The code is written in the MATLAB language and runs in the MATLAB environment. The code has been implemented in two versions, applied to
(1) Horizontal low-frequency (100 to 500 Hz) propagation through the shallow water waveguide environment;
(2) Vertical high-frequency propagation (6 to 15 kHz) to study normal-incidence reflection from the lower side of the ocean surface.
The first edition of the code reported on here does not implement refinements that are often found in 2D propagation models, such as allowing density to vary, optimally smoothing sound-speed discontinuities at the water/seabed interface, and allowing an omni-directional source. The code is part of a development effort to test the applicability of 2D (and N by 2D) models, which have more refinements than this model, to the study of fully 3D propagation problems, such as sound transiting steep nonlinear coastal-area internal waves and/or sloping terrain, and to provide a numerical tool when the full 3D solution is needed.

17. Document Analysis **a. Descriptors**

Acoustics
Numerical simulation
Fourier split step

b. Identifiers/Open-Ended Terms

c. COSATI Field/Group

18. Availability Statement	19. Security Class (This Report)	21. No. of Pages
Approved for public release; distribution unlimited.	UNCLASSIFIED	20
	20. Security Class (This Page)	22. Price

(See ANSI-Z39.18) *See Instructions on Reverse*

OPTIONAL FORM 272 (4-77)
(Formerly NTIS-35)
Department of Commerce